B cell profiles, antibody repertoire and reactivity reveal dysregulated responses with autoimmune features in melanoma

Authors: Silvia Crescioli[1], Isabel Correa[1], Joseph Ng[2,3], Zena N. Willsmore[1], Roman Laddach[1,4], Alicia Chenoweth[1,5], Jitesh Chauhan[1], Ashley Di Meo[6], Alexander Stewart[7], Eleni Kalliolia[1], Elena Alberts[5], Rebecca Adams[1], Robert J. Harris[1], Silvia Mele[1], Giulia Pellizzari[1], Anna B. M. Black[1], Heather J. Bax[1], Anthony Cheung[1,5], Mano Nakamura[1], Ricarda M. Hoffmann[1], Manuela Terranova-Barberio[1], Niwa Ali[8,9], Ihor Batruch[6], Antoninus Soosaipillai[6], Ioannis Prassas[6], Antigona Ulndreaj[6], Miyo K. Chatanaka[6,10], Rosamund Nuamah[11], Shichina Kannambath[11,12], Pawan Dhami[11], Jenny L. C. Geh[13,14], Alastair D. MacKenzie Ross[14], Ciaran Healy[14], Anita Grigoriadis[5], David Kipling[7], Panagiotis Karagiannis[1,15], Deborah K Dunn-Walters[7], Eleftherios P. Diamandis[6,10,16,17], Sophia Tsoka[4], James Spicer[18], Katie E. Lacy[1], Franca Fraternali[2,3], Sophia N. Karagiannis[1,5]*.

Affiliations:

[1] St John's Institute of Dermatology, School of Basic & Medical Biosciences, King's College London, Guy's Hospital; London, United Kingdom

[2] Randall Centre for Cell and Molecular Biophysics, King's College London; London, United Kingdom

[3] Research Department of Structural and Molecular Biology, University College London; London, United Kingdom

[4] Department of Informatics, Faculty of Natural, Mathematical and Engineering Sciences, King's College London; London, United Kingdom

[5] Breast Cancer Now Research Unit, School of Cancer & Pharmaceutical Sciences, King's College London, Guy's Hospital; London, United Kingdom

[6] Lunenfeld-Tanenbaum Research Institute, Mount Sinai Hospital; Toronto, Canada

[7] School of Biosciences and Medicine, University of Surrey; Guildford, United Kingdom

[8] Peter Gorer Department of Immunobiology, School of Immunology and Microbial Sciences, Faculty of Life Sciences and Medicine, King's College London, London, UK

[9] Centre for Gene Therapy and Regenerative Medicine, School of Basic and Medical Biosciences, Faculty of Life Sciences and Medicine, King's College London, London, UK

[10] University of Toronto, Department of Laboratory Medicine and Pathobiology; Toronto, Canada

[11] Biomedical Research Centre, Guy's and St. Thomas' NHS Foundation Trust; London, United Kingdom

[12] Genomics Facility, Institute of Cancer Research; London, United Kingdom

[13] St John's Institute of Dermatology, Guy's, King's, and St. Thomas' Hospitals NHS Foundation Trust; London, United Kingdom

[14] Department of Plastic Surgery at Guy's and St. Thomas' NHS Foundation Trust; London, United Kingdom

[15] Department of Cancer Biology, Dana-Farber Cancer Institute, Boston, MA, USA.

[16] Department of Pathology and Laboratory Medicine, Mount Sinai Hospital; Toronto, Canada

[17] Department of Clinical Biochemistry, University Health Network; Toronto, Canada

[18] School of Cancer & Pharmaceutical Sciences, King's College London, Guy's Hospital; London, United Kingdom

*Corresponding author: Sophia N. Karagiannis, E-mail: sophia.karagiannis@kcl.ac.uk

Supplementary Information

Supplementary Figure 1

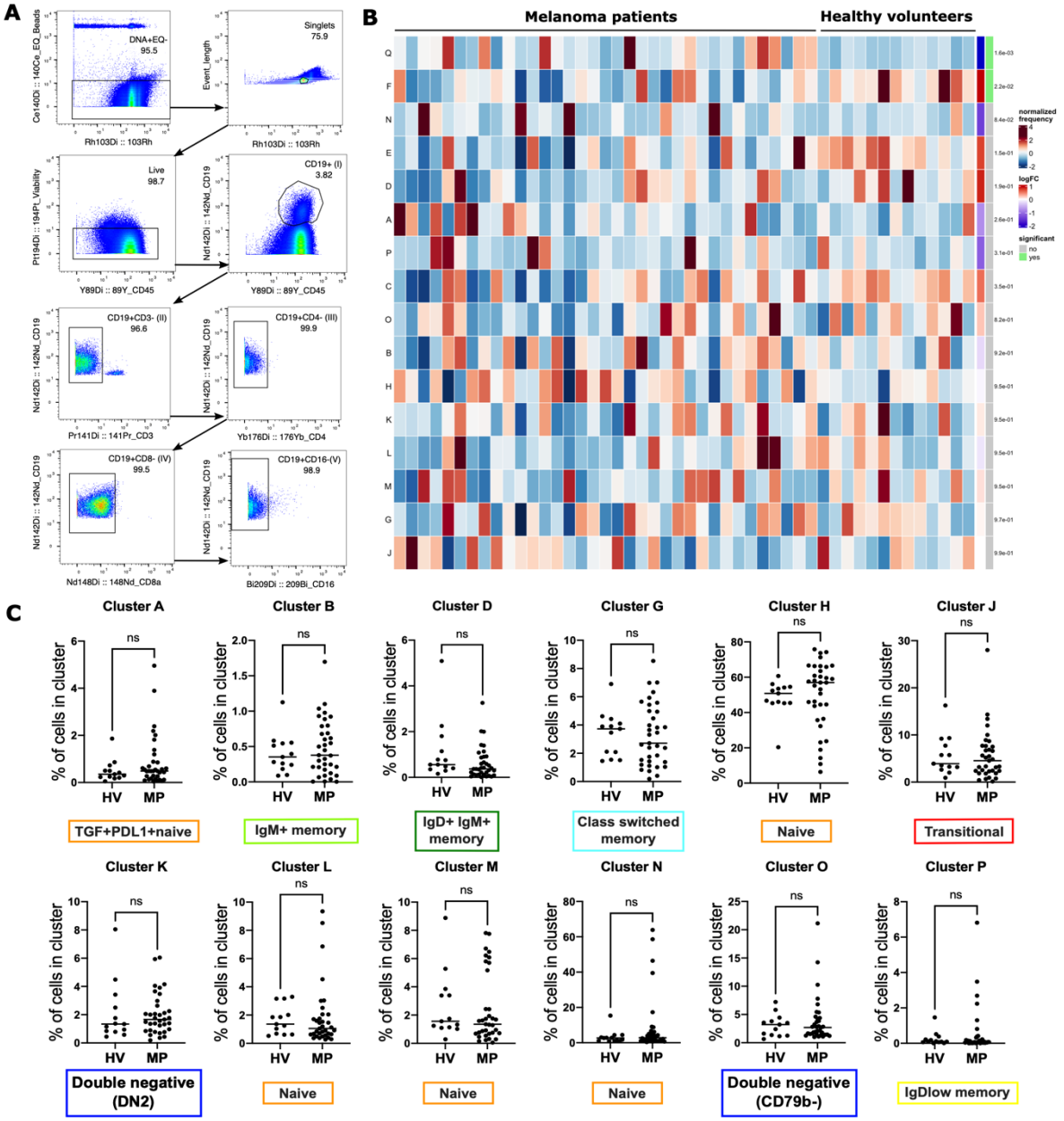

Supplementary Figure 1: Gating strategy and differential abundance analysis to compare healthy volunteers and melanoma patients. (**A**) CyTOF gating strategy to identify B cell subsets for analysis. (B-C) biologically independent samples: Healthy volunteers, n = 13; Melanoma patients, n = 35. (**B**) Differential Abundance analysis (DA test) comparing healthy volunteer and melanoma patient samples. (**C**) Scatter dot plot showing the non-significant comparisons of the relative abundance of B cell clusters in each sample between healthy

volunteers and melanoma patients. Statistical significance was calculated with the Mann-Whitney test.

Supplementary Figure 2

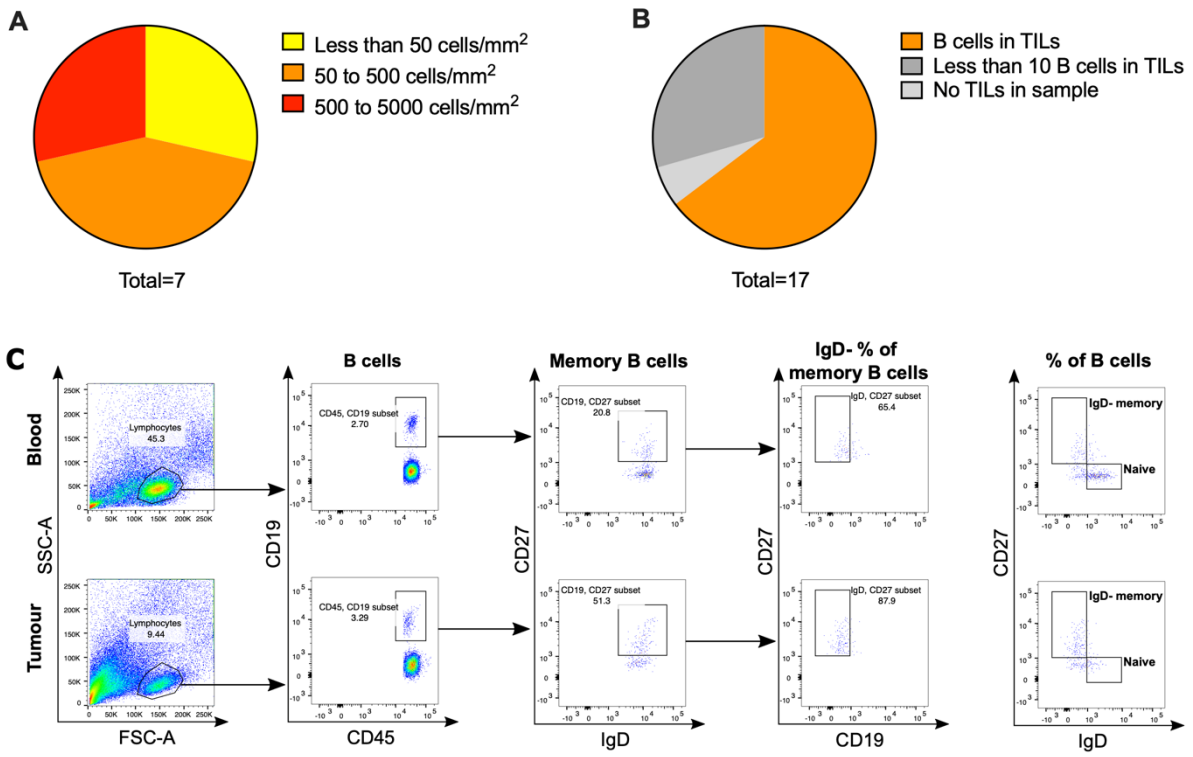

Supplementary Figure 2: B cell infiltration in cutaneous melanoma metastases. (**A**) Pie chart representing the presence and density of CD20+ B cells in tumor samples (intratumoral and peritumoral) analyzed by immunofluorescence (n = 7). The numbers of CD20+ B cells per mm^2 were calculated using QuPath software. (**B**) Pie chart representing the presence of B cells (CD19+ cells) in Tumor infiltrating Lymphocytes (TILs) (CD45+ cells) in the 17 tumor samples analyzed by flow cytometry. (**C**) Flow cytometry gating strategy for B cell phenotyping in melanoma patient blood and tumor samples.

Supplementary Figure 3

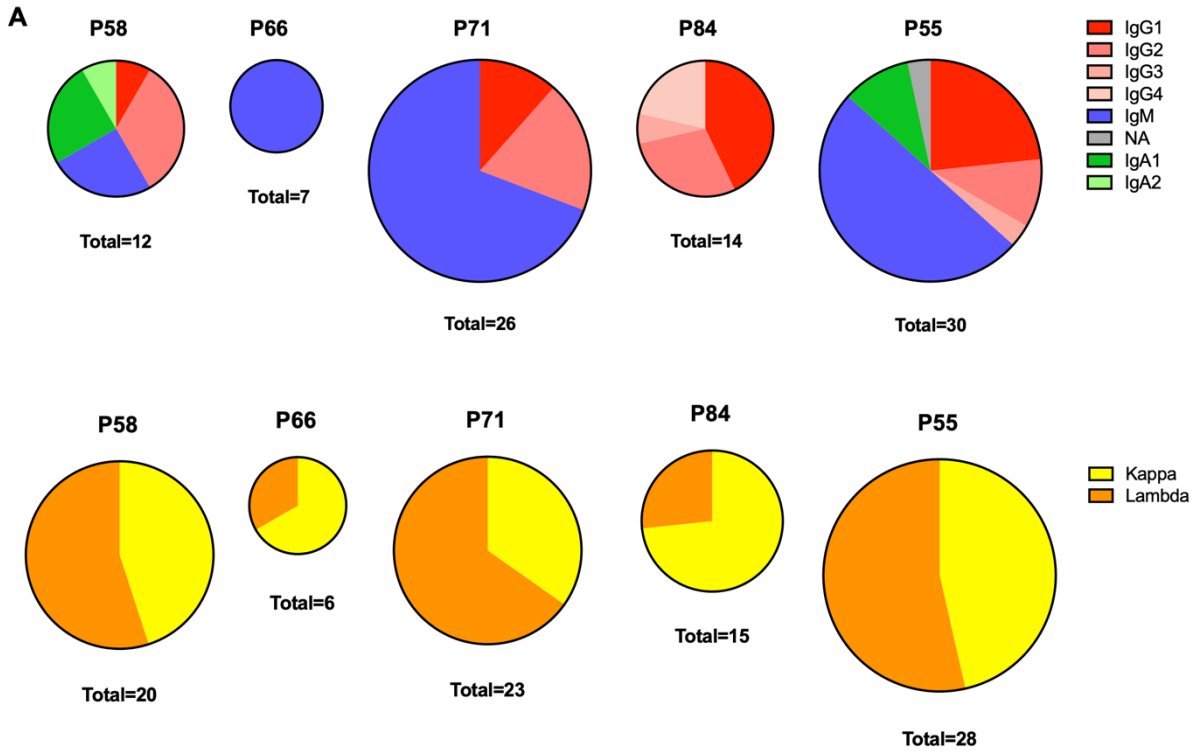

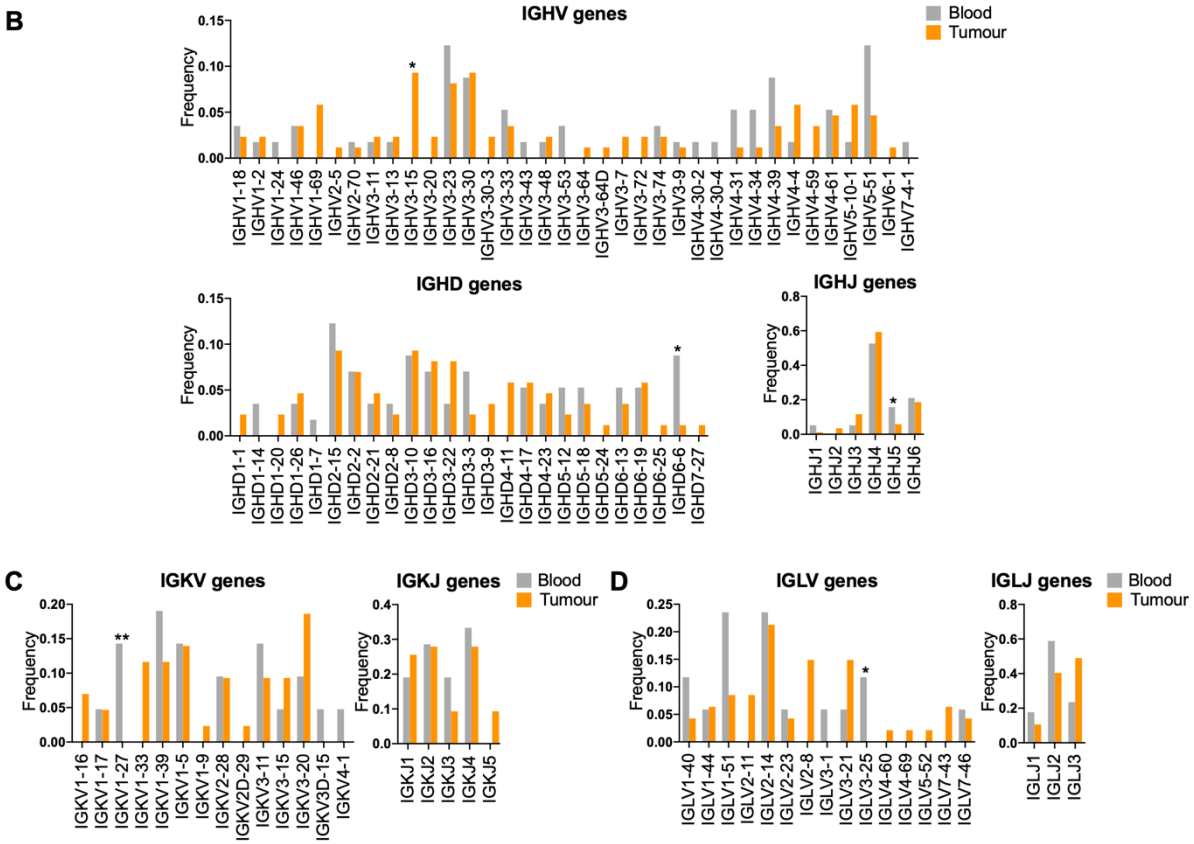

Supplementary Figure 3: Antibody repertoire on IgD- memory B cells isolated from melanoma patient blood and tumor samples. (**A**) Pie charts representing the isotype distribution per patient; the values below each chart depict the numbers of heavy chain sequences per patient. (**B-D**) Comparison between melanoma patients' blood (grey, n = 11; 57 heavy chain and 38 light chain sequences) and tumor (orange, n = 5; 89 heavy chain and 92 light chain sequences). (**B**) Frequency distribution of heavy chain IGHV, IGHD and IGHJ genes. (**C**) Frequency distribution of kappa light chain IGKV and IGKJ genes and (**D**) lambda light chain IGLV and IGLJ genes. Statistical significance was calculated with a two-sample proportion z-test; *P < 0.05, **P < 0.01.

Supplementary Figure 4

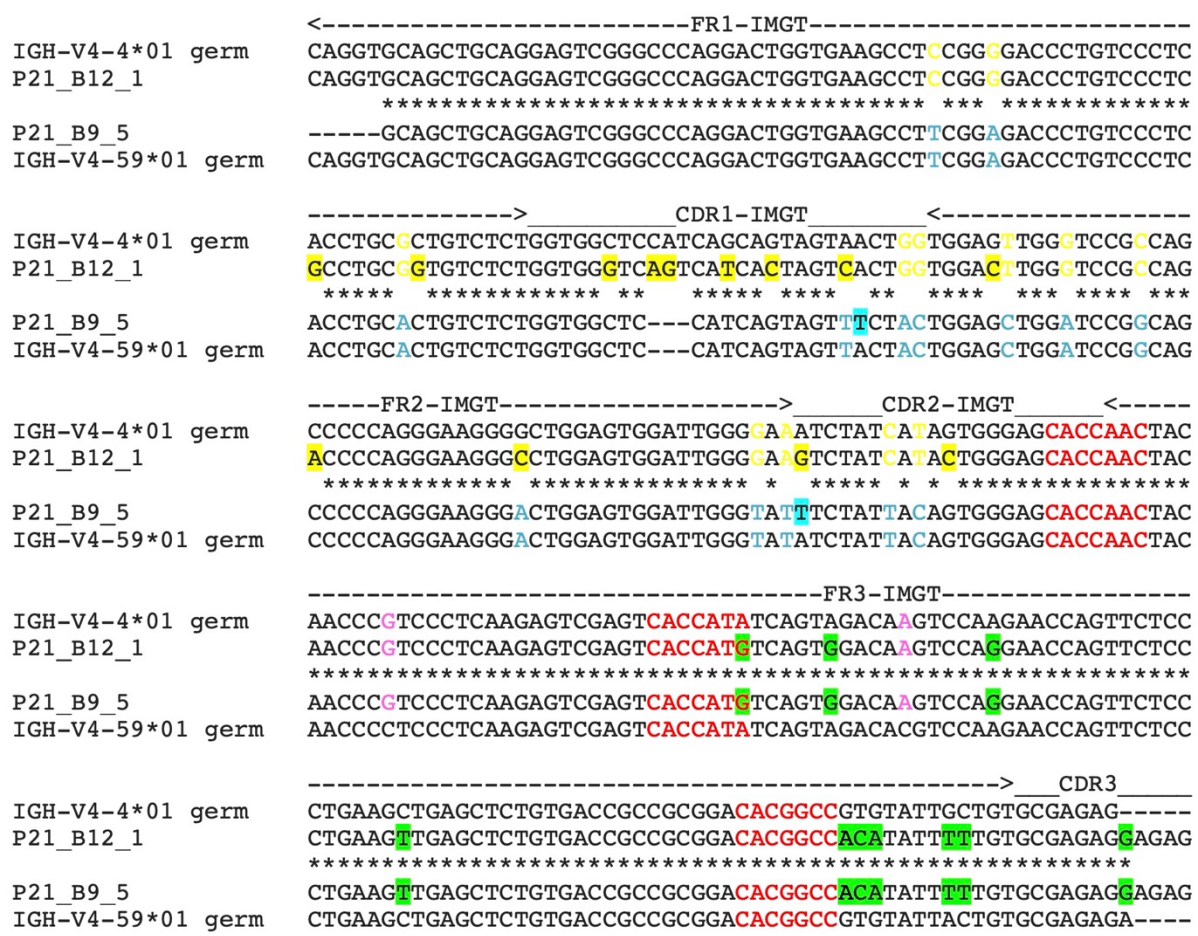

Supplementary Figure 4: VH replacement. cDNA VH sequence alignment of the example in Figure 5E (M847_IgG_B12_1 and M847_IgG_B9_5 clones and germlines) with Frameworks and CDRs annotation according to IMGT. Asterisks: identical nucleotides in clones; Purple font: identical nucleotides in clones and germline IGH-V4-4*01 only; Yellow font: identical nucleotides in M847_IgG_B12_1 and germline IGH-V4-4*01 only; Blue font: identical nucleotides in M847_IgG_B9_5 clone and germline IGH-V4-59*01 only; Yellow highlight: unique nucleotides in M847_IgG_B12_1 clone; Light blue highlight: unique nucleotides in M847_IgG_B9_5 clone; Green highlight: nucleotides in both clones but not in germlines; Red font: possible heptamer site for recombination.

Supplementary Figure 5

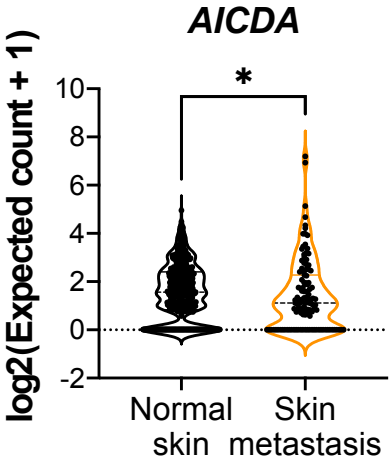

Supplementary Figure 5: *AICDA (AID)* gene expression in cutaneous samples. *AICDA (AID)*, gene expression in normal skin (n = 555) and melanoma skin metastases (n = 116) (RSEM expected count (DESeq2 standardized) dataset, TCGA TARGET GTEx study, UCSC Xena).

Supplementary Figure 6

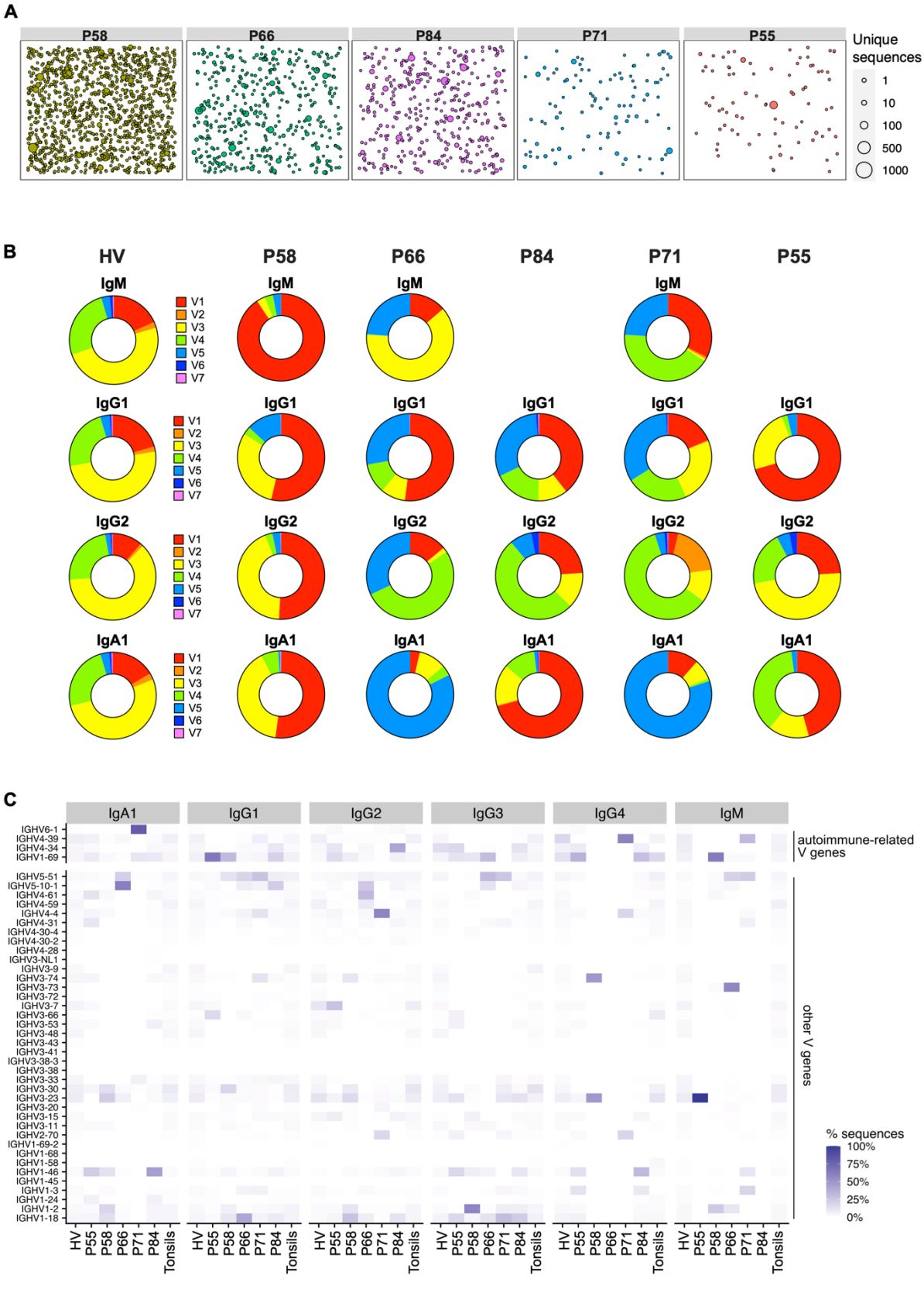

Supplementary Figure 6: V gene distribution per antibody isotype. (**A**) Representation of IgH clones and clonal expansion per tumor sample: the circle size is proportional to the number of unique sequences per clone. (**B**) Pie charts representing V family distribution in healthy volunteers (HV) and melanoma patients (MP) per isotype, divided per tumor sample. (**B**) Heatmap representing V gene proportions for each antibody isotype detected in each tumor sample in comparison with the average of healthy volunteer blood and tonsil samples V family distribution. The top 4 V genes have been associated with autoimmunity[1].

Supplementary Figure 7

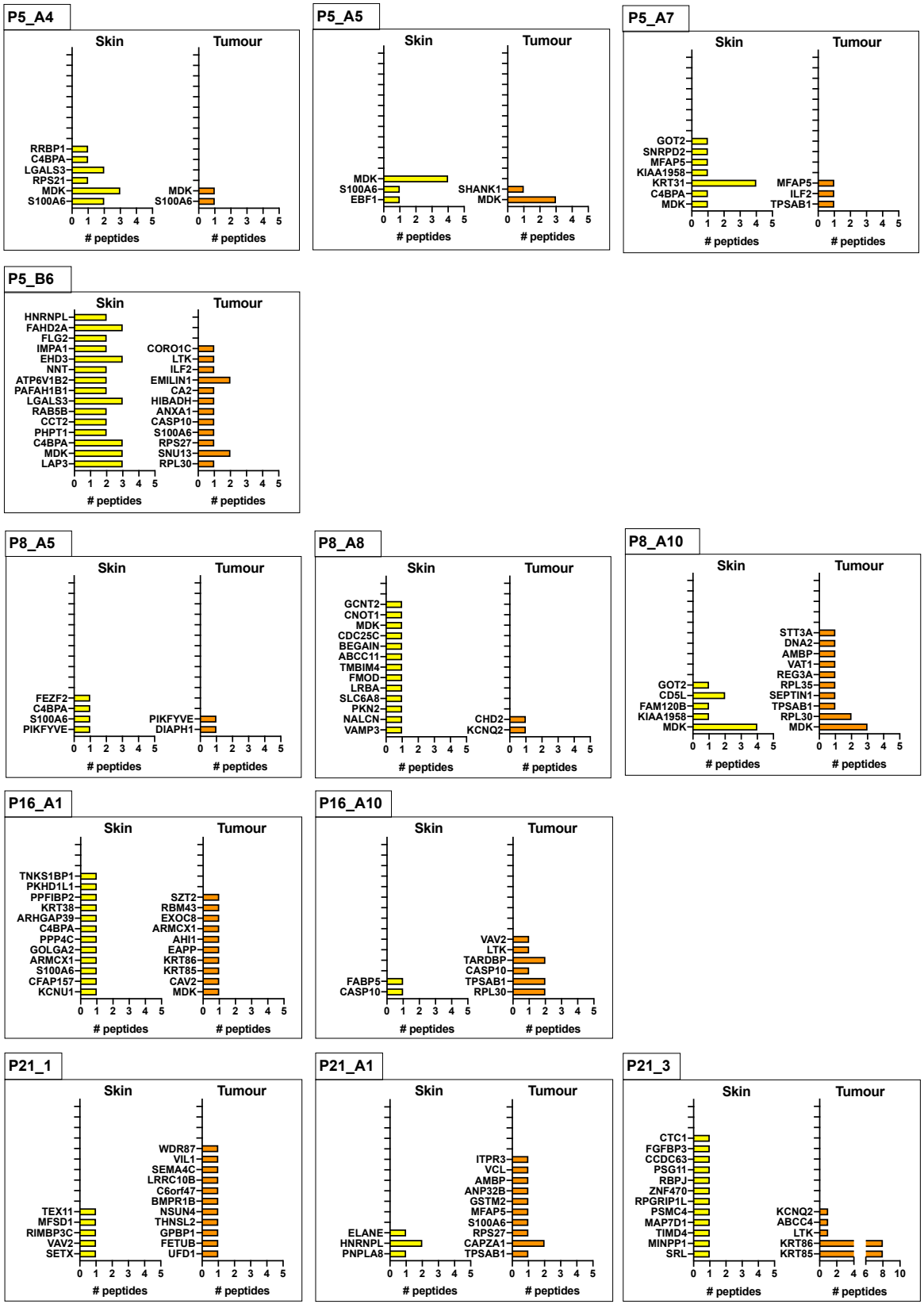

Supplementary Figure 7: Immuno-mass spectrometry via Shotgun Mass-Spectrometry LC-MS/MS. Bar charts representing, for every antibody, the proteins identified in the immuno-mass spectrometry via Shotgun Mass-Spectrometry LC-MS/MS in Normal Skin and Melanoma Tumor. In the histograms is shown the number of peptides identified for each protein.

Supplementary Figure 8

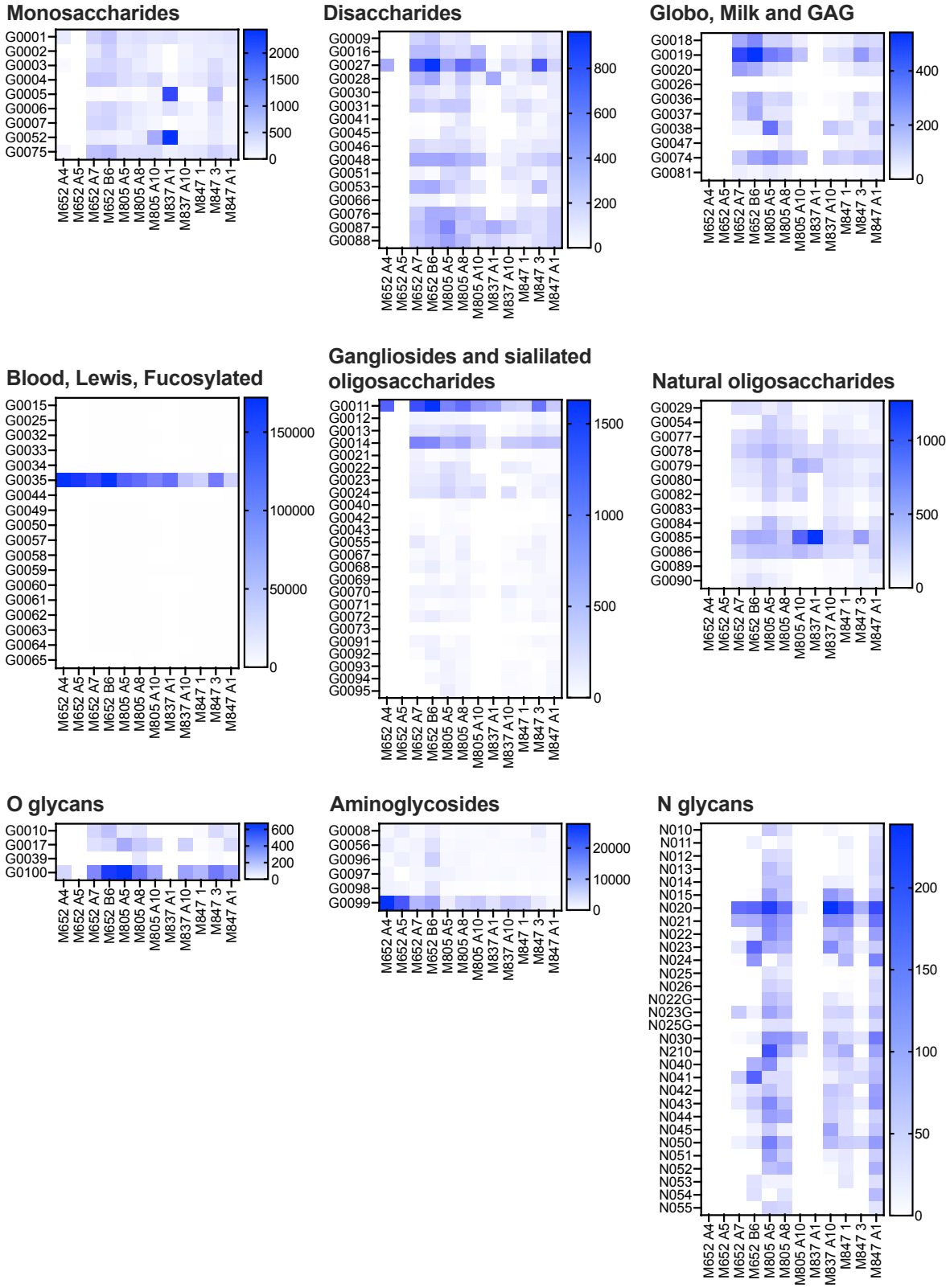

Supplementary Figure 8: Glycan array heatmap 1. Heatmap representing the analyzed glycan array results grouped the glycans classes according to Glycan Array 300 manufacturers: "Monosaccharides", "Disaccharides", "Globo, Milk and GAG", "Blood, Lewis, Fucosylated", "Gangliosides and sialylated oligosaccarides", "Natural oligosaccharides", "O glycans", "Aminoglycosides", "N glycans".

Supplementary Figure 9

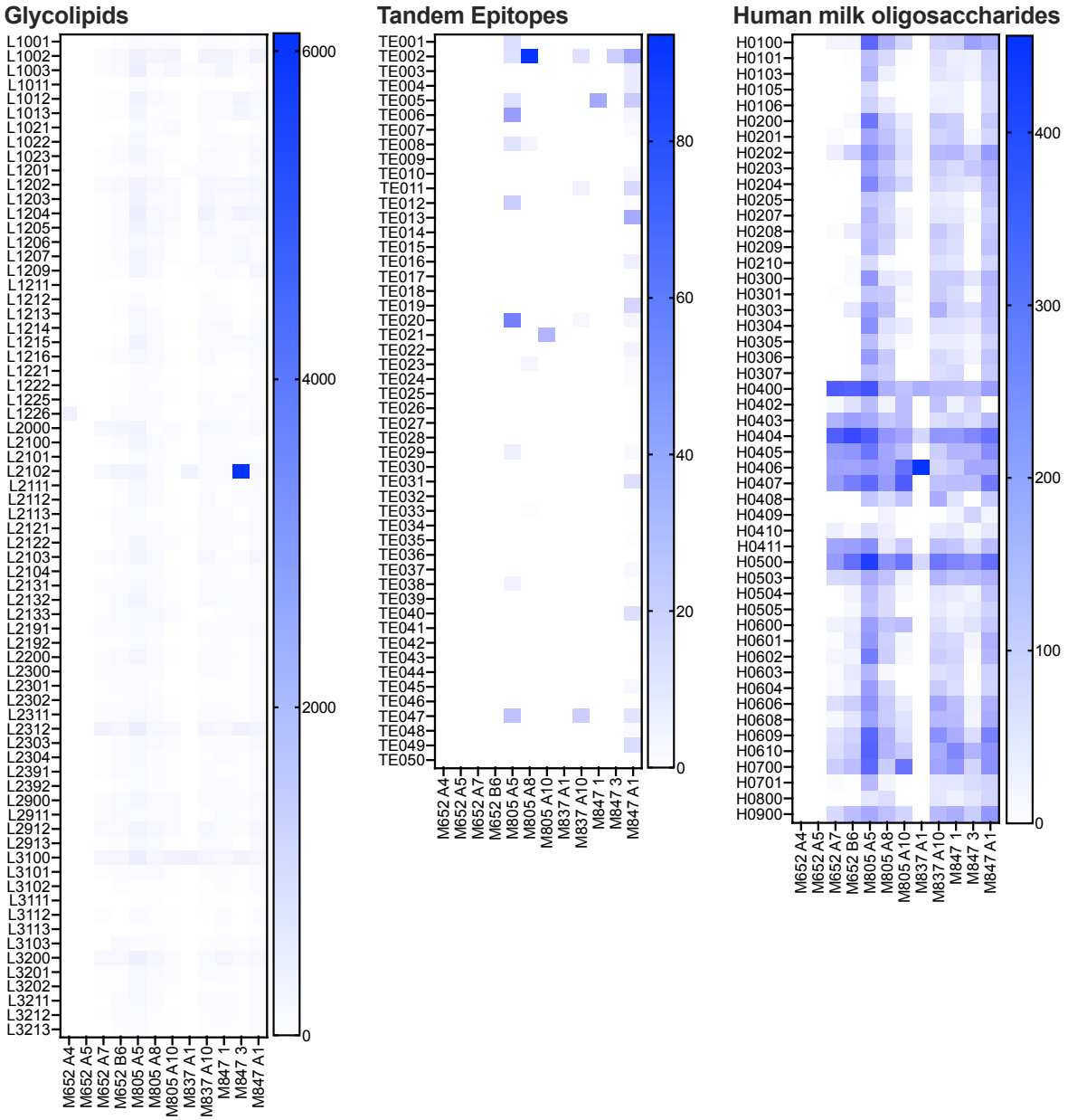

Supplementary Figure 9: Glycan array heatmap 2. Heatmap representing the analyzed glycan array results grouped the glycans classes according to Glycan Array 300 manufacturers: "Glycolipids", "Tandem Epitopes", "Human milk oligosaccharides".

Supplementary Figure 10

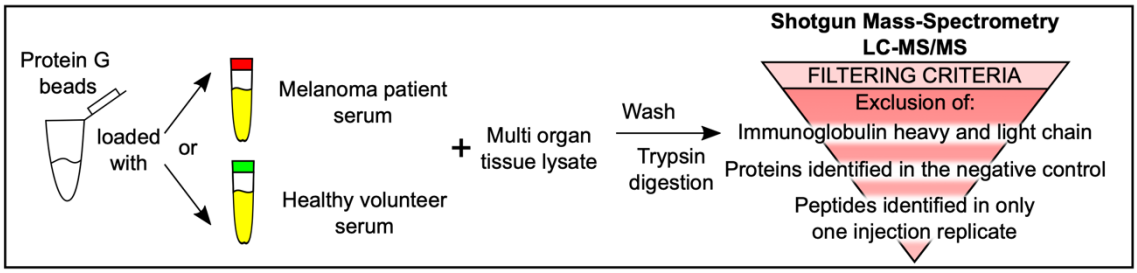

Supplementary Figure 10: Serum immuno-mass spectrometry study pipeline. Schematic of immuno-mass spectrometry workflow for patient and healthy volunteer serum sample analysis.

Supplementary Figure 11

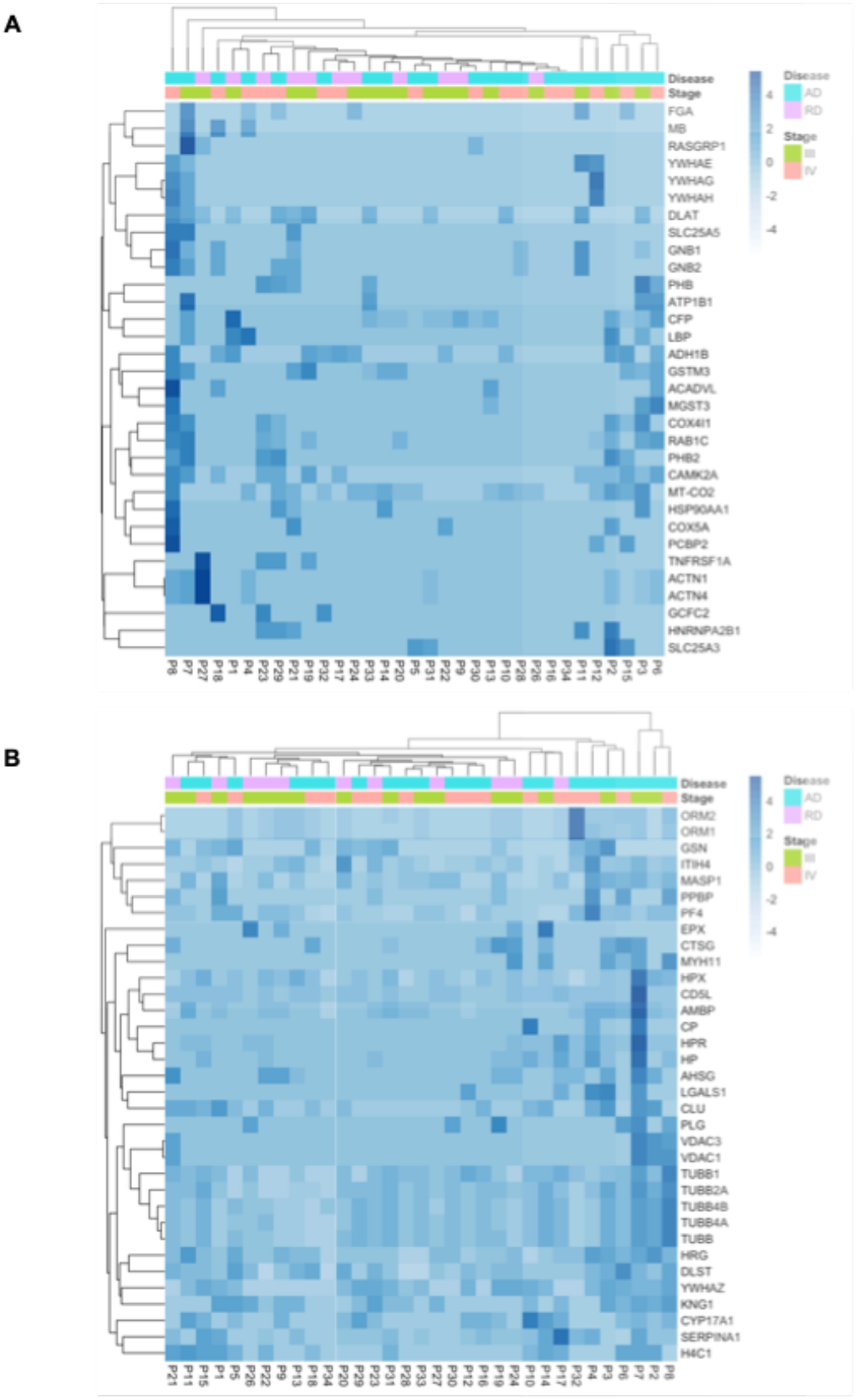

Supplementary Figure 11: Heatmap of serum immuno-mass spectrometry (IMS) peak area. Heatmap of immuno-mass spectrometry (IMS) peak area annotated with information on stage (III or IV) and active (AD) or resected (RD) disease status, for autoantibodies found in melanoma patients only (A) and in both melanoma patients and healthy volunteers (B) serum.

Supplementary Figure 12

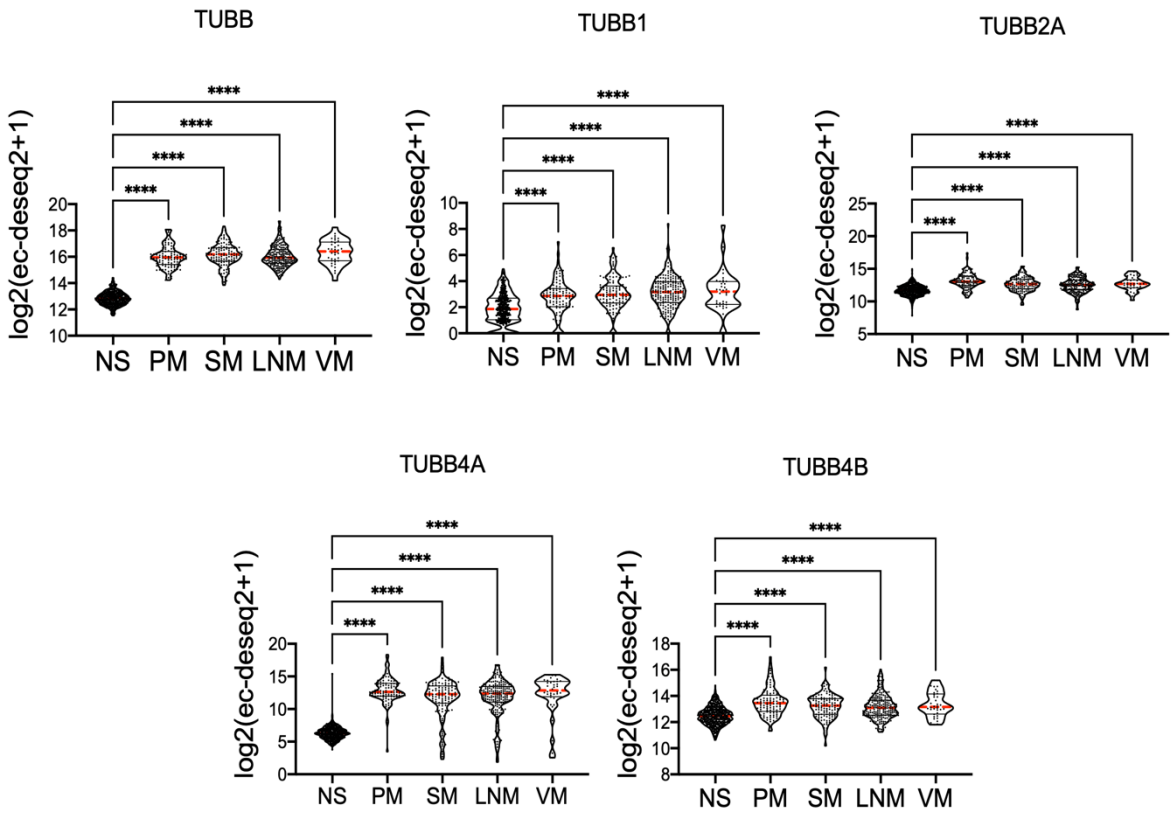

Supplementary Figure 12: Gene expression of tubulins in human skin and melanoma lesions. Gene expression of TUBB, TUBB1, TUBB2A, TUBB4A, TUBB4B in: normal skin, NS (n = 555); primary melanoma, PM (n = 102); melanoma skin metastases, SM (n = 116); lymph node metastases, LNM (n = 208); visceral metastases, VM (n = 36); (RSEM expected count (DESeq2 standardized) dataset, TCGA TARGET GTEx study, UCSC Xena). Statistical significance was calculated with non parametric ANOVA (Kruskal-Wallis test); *P < 0.05, **P < 0.01, ***P < 0.001 and ****P < 0.0001.

Supplementary Figure 13

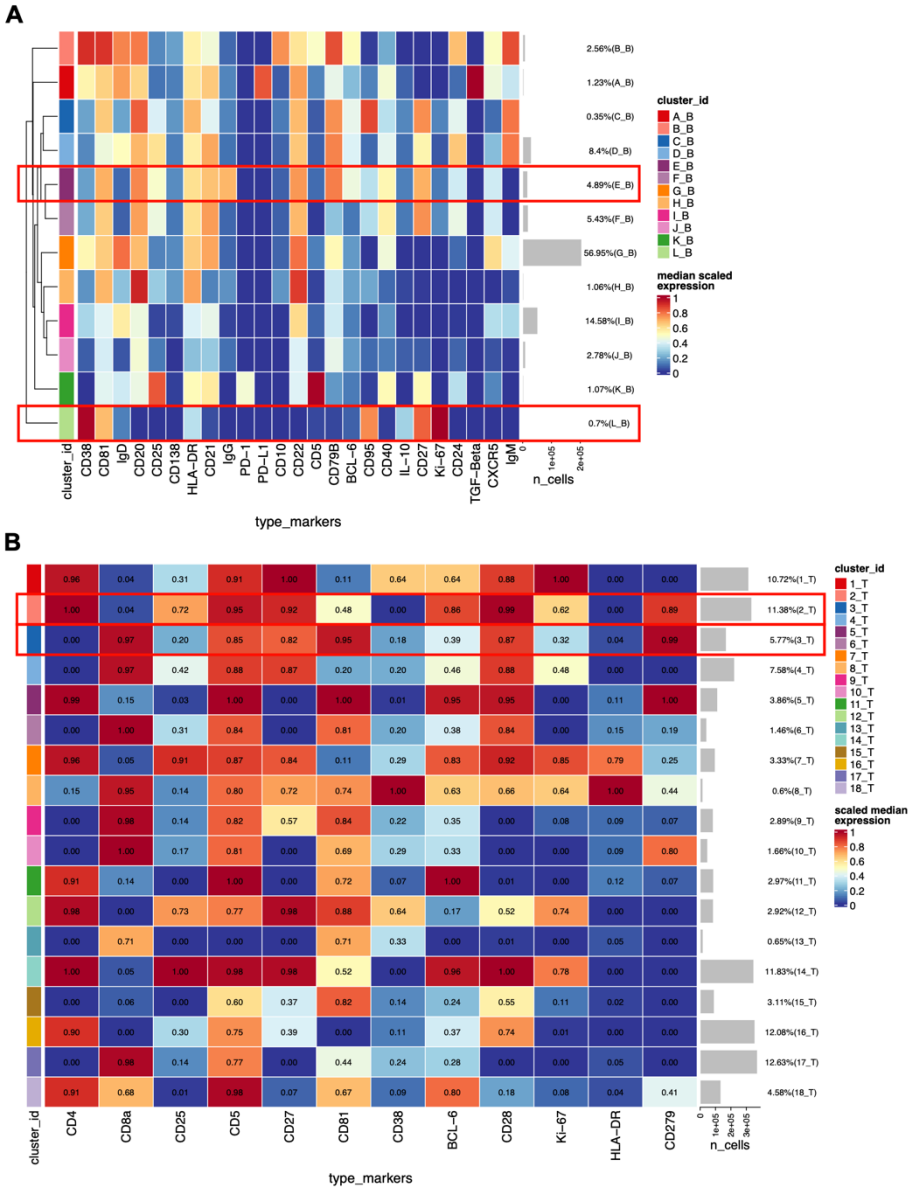

Supplementary Figure 13: Heatmaps of marker expression for B cells and T cells detected by CyTOF analyses in melanoma patient blood samples. Heatmaps represent the median scaled expression of the markers used for B cell (**A**) or T cell (**B**) clustering. Red rectangles indicate the clusters of interest.

Supplementary Table 1: Criteria used for labelling and merging CyTOF clusters [2].

Cluster	Markers	Population
A	CD27- IgD++ IgMlow CD38+ CD24- TGFβ + PDL1+	Naïve TGFβ+ PDL1+
B	CD27+ IgD- IgM++ CD38low CD24+	IgM+ memory
C	CD27+ IgD+ IgM++ CD38+/- CD24+	IgD+ IgM+ memory
D	CD27+ IgD+ IgM++ CD38+/- CD24- CD21- CD95- BCL6+	IgD+ IgM+ memory
E	CD27+ IgD- IgM- IgGlow CD38+/- CD24+ CD21+ CD95+/-	Class switched memory (resting)
F	CD27- IgD- IgM- IgG++ CD38+ CD24low CD21+ CXCR5+	Double negative (DN1)
G	CD27+ IgD- IgM- IgG- CD38+/- CD24- CD21+ CD95++ CD79Blow	Class switched memory (activated)
H	CD27- IgD+ IgMlow CD38+ CD24- CD21+ CD95-	Naïve
J	CD27- IgD++ IgM++ CD38++ CD24+ CD10+	Transitional
K	CD27- IgD- IgM- IgG++ CD38+/- CD24- CD21- CXCR5-	Double negative (DN2)
L	CD27- IgM+/- IgD++ CD24- CD38- CD21-	Naïve (activated)
M	CD27+/- IgM+ IgD+/- CD24+/- CD38-	Naïve
N	CD27- IgM+/- IgD+ CD24- CD38+/- CXCR5+	Naïve
O	CD27- IgM- IgD- CD24- CD38+/- CD79-	Double negative (CD79b-)
P	CD27+ IgG- IgM- IgD+/- CD24+/- CD38- CD21+ CD5+++ CD25+++ PD1+ CD79B-	IgDlow memory
Q	CD27+++ IgG- IgM- IgD- CD24- CD38+++ CD95++ ki67+++ CD79B-	Plasmablasts

Supplementary Table 2: Number of sequences per melanoma skin metastasis sample derived in high throughput antibody repertoire analyses.

Donor	Number of total sequences			
	IgH	IgK	IgL	Number of IgH clones
P55	21,312	4,929	5,404	82
P58	87,565	83,417	86,190	1263
P66	67,144	78,023	77,111	443
P71	5,605	5,204	6,708	104
P84	43,389	13,558	14,220	994

Supplementary Table 3: Number of heavy chain sequences derived per cohort in high throughput antibody repertoire.

Cohort	Number of samples	Number of unique sequences
HV (Healthy Volunteer)	9	68,347
MP (Melanoma Patient)	5	27,506
EB (ebola)	12	60,020
Covid-19	16	331,159
Tonsils	8	1,429,393

Supplementary Table 4: Melanoma patients recruited for PBMC analysis by CyTOF.

Sample code	Gender	Age	Stage at sampling
P2	M	85	IIIC
P3	M	88	IIIC
P4	M	78	IV
P7	M	86	IIIC
P8	F	75	IV
P10	F	78	IV
P11	M	79	IIIB
P12	F	79	IV
P13	F	64	IIIC
P14	F	82	IIID
P15	M	77	IV
P16	M	80	IV
P18	M	73	IV
P23	F	77	IV
P24	F	64	III
P26	F	69	IIIC
P27	M	60	IIIC
P32	M	67	IV
P33	M	57	IIIC
P35	F	76	IIIB
P36	M	81	IV
P37	M	85	IV
P38	F	65	III
P39	M	72	IIIC
P40	F	85	IV
P41	F	79	IIIC
P42	M	77	IV
P43	M	61	IIIC
P44	F	65	IV
P45	F	80	IIIC
P46	M	71	IV
P47	F	68	IV
P48	F	68	IV
P49	M	74	III
P50	F	83	IIIC

Supplementary Table 5: Healthy volunteers recruited for PBMC analysis by CyTOF.

Sample code	Gender	Age
HV1	F	59
HV2	F	72
HV3	F	68
HV4	M	35
HV5	M	76
HV6	F	77
HV7	F	72
HV8	F	55
HV9	F	61
HV10	F	59
HV11	F	88
HV12	F	37
HV13	M	28

Supplementary Table 6: Melanoma patients recruited for PBMC analysis by Flow Cytometry.

Sample code	Gender	Age	Stage at sampling
P51	M	56	IV
P52	F	44	IIIC
P53	F	77	IIIA
P54	M	41	IV
P55	M	66	IV
P56	M	45	IV
P57	M	47	IV
P58	F	67	IIIC
P59	M	48	IV
P60	M	65	IV
P61	M	60	IV
P62	F	81	IV
P63	M	47	IIIC
P64	F	59	IV
P65	F	84	III
P66	M	80	IIIB
P67	M	70	IV
P68	M	31	IV
P69	F	71	IV
P70	M	59	IIIC
P71	F	60	IV
P72	F	80	IIB
P73	F	77	IIIB
P74	M	74	IIIC
P75	M	89	IV
P76	F	80	IV
P77	F	83	IIIC
P78	M	95	IIIB
P79	M	77	IIIC

Supplementary Table 7: Melanoma lesion specimens.

Sample code	Age	Gender	Stage	Lesion type	Reason for exclusion from the analysis	TILs* in original primary melanoma
P55-1	53	F	IIIB	Subcutaneous metastasis		Present: non-brisk
P55-2	54	F	IIIB	In transit melanoma		Present: non-brisk
P56	45	M	IV	Cutaneous primary lesion		N/A
P57	61	F	IIIC	Cutaneous metastasis		Absent
P58	76	F	IIC	Subcutaneous in-transit metastasis		Absent
P59	49	M	IIB	Desmoplastic melanoma, primary lesion		Present: non brisk from desmoplastic lesion
P66	76	M	IV	Subcutaneous metastasis		Present: non-brisk
P71	70	M	IV	Subcutaneous metastasis		Present: non-brisk
P77	80	F	IIB	Subcutaneous in-transit metastasis	less than 10 B cells	N/A
P79	74	M	IIIC	Subcutaneous in-transit metastasis	less than 10 B cells	Present: non-brisk
P80	80	F	IV	Subcutaneous in-transit metastasis		Present: non-brisk
P81	83	F	IIIC	Subcutaneous in-transit metastasis	less than 10 B cells	Absent
P82	95	M	IIIB	Subcutaneous in-transit metastasis		Present: non-brisk
P83	77	M	IIIC	Subcutaneous in-transit metastasis	less than 10 B cells	Present: non-brisk
P84	66	F	IIA	Cutaneous metastasis		Present: non-brisk
P85	M	F	IB	Primary cutaneous melanoma	No TILs in sample	N/A
P86	70	F	IV	Recurrent subcutaneous metastasis	less than 10 B cells	Present: non-brisk
P87	84	M	IV	Subcutaneous in-transit metastasis	No memory B cells in TILs	Present: non-brisk

* TILs: tumor infiltrating lymphocytes

Supplementary Table 8: Melanoma patients recruited for serum immuno-mass spectrometry analysis.

Sample code	Gender	Age	Stage at sampling	Autoimmune related co-morbidities
P1	M	57	IIIB	
P2	M	85	IIIC	Ulcerative colitis
P3	M	88	IIIC	
P4	M	78	IV	
P5	F	35	IV	
P6	F	35	IV	
P7	M	86	IIIC	
P8	F	75	IV	
P9	M	58	IIIC	
P10	F	78	IV	
P11	M	79	IIIB	
P12	F	79	IV	
P13	F	64	IIIC	
P14	F	82	IIID	
P15	M	77	IV	Baseline autoimmune thyroid disease
P16	M	80	IV	
P17	M	57	IV	
P18	M	73	IV	
P19	M	83	IIIC	
P20	F	72	IIIC	
P21	M	49	IIIB	
P22	M	44	IIIA	
P23	F	77	IV	
P24	F	64	III	
P26	F	60	IIIC	Baseline autoimmune thyroid disease, polymyalgia rheumatica
P27	F	69	IIIC	
P28	M	60	IIIC	
P29	M	60	IV	
P30	F	65	IV	
P31	M	83	IV	
P32	F	80	IIIC	
P33	M	67	IV	
P34	M	57	IIIC	

Supplementary Table 9: CyTOF antibody panel.

Metal Tag	Antibody	Clone	Source
89Y	CD45	HI30	Fluidigm
141Pr	CD3	UCHT1	Fluidigm
142Nd	CD19	HIB19	Fluidigm
144Nd	CD38	HIT2	Fluidigm
145Nd	CD81	5A6	Fluidigm
146Nd	IgD	IA6-2	Fluidigm
147Sm	CD20	2H7	Fluidigm
148Nd	CD8a	SK1 (Custom)	Biolegend
149Sm	CD25 (IL2R)	2A3	Fluidigm
150Nd	CD138	DL-101	Fluidigm
151Eu	HLA-DR	G46-6	Fluidigm
152Sm	CD21	BL13	Fluidigm
153Eu	Ig Lambda	MHL-38 (Custom)	Biolegend
154Sm	IgG R10	R10 (Custom)	RND
155Gd	CD279 (PD-1)	EH12.2H7	Fluidigm
156Gd	CD274 (PD-L1)	29E.2A3	Fluidigm
158Gd	CD10	HI10a	Fluidigm
159Tb	CD22	HIB22	Fluidigm
160Gd	Ig Kappa	MHK-49	Fluidigm
161Dy	CD5	UCHT2 (Custom)	Biolegend
162Dy	CD79B	CB3-1	Fluidigm
163Dy	BCL-6	K112-91	Fluidigm
164Dy	CD95/Fas	DX2	Fluidigm
165Ho	CD40	5C3	Fluidigm
166Er	IL-10	JES3-9D7	Fluidigm
167Er	CD27	L128	Fluidigm
168Er	Ki-67	B56	Fluidigm
169Tm	CD24	ML5	Fluidigm
170Er	TGF-Beta	TW4-6H10 (Custom)	Biolegend
171Yb	CD185 (CXCR5)	51505	Fluidigm
172Yb	IgM	MHM-88	Fluidigm
175Lu	CD28	CD28.2 (Custom)	Biolegend
176Yb	CD4	RPA-T4	Fluidigm
209Bi	CD16	3G8	Fluidigm

Supplementary Methods

Immuno-mass spectrometry

Tissue protein extraction: Fresh frozen skin (n = 3) and melanoma (n = 2) tissue sections collected at autopsy or surgery, respectively. Samples were cut and weighed (~500-700 mg wet weight). Tissues were individually pulverized in liquid nitrogen with a mortar and pestle to yield a fine powder. Proteins were extracted and solubilized using 0.2% RapiGest (Waters Corporation, Milford, USA) in 50 mM ammonium bicarbonate (ABC). The pulverized tissue samples were vortexed every 5 minutes on ice, for 30 minutes, and then sonicated on ice three times for 15 s with the MISONIX immersion tip sonicator (Q SONICA LLC, CT, USA). The tissue samples were centrifuged at 15,000 x g at 4°C for 20 minutes and the supernatant was collected. A Pierce BCA Protein Assay (Thermo Fisher Scientific, San Jose, California) was performed on each tissue protein extract for total protein quantification. Melanoma tissue lysates were pooled in equal parts (in terms of total protein contribution).

Monoclonal IgG antibody immunoprecipitation: Unknown IgG monoclonal antibodies (n = 12) were purified using protein G magnetic beads (Protein G Mag Sepharose Xtra, GE Healthcare, Chicago, USA). Briefly, 50 µl of 10% w/v medium slurry was resuspended and added to each microcentrifuge tube. The storage solution was removed using a magnetic particle concentrator (MPC-E, Dynal, Oslo, Norway). The magnetic beads were then equilibrated with 500 µl of 1X PBS. Following the removal of the 1X PBS solution, 50 µl of each unknown IgG monoclonal antibody (1 µg/µl) was diluted to a final volume of 300 µl using 1X PBS and added to the magnetic beads. CSPG4 and NIP monoclonal antibodies served as a positive and negative control, respectively and were processed separately from the unknown IgG monoclonal antibodies. Samples were incubated for 30-minutes with gentle rotation. The magnetic beads were then washed twice with 500 µl 1X PBS and incubated with 100 µg of pooled melanoma

tissue lysate for 2 hours with gentle rotation. The magnetic beads were then washed two times with 500 µl 1X PBS 0.05% Tween 20. This was followed by an additional two washes with 500 µl 1X PBS. The beads were resuspended in 100 µl of PBS for on-bead trypsin digestion. The immuno-captured monoclonal antibodies and their cognate target antigens were reduced with 100 mM DTT added to a final concentration of 5 mM and incubated for 40 minutes at 56°C. The samples were then alkylated with 500 mM IAA added to a final concentration of 15 mM and incubated for 30 minutes at room temperature, in the dark and with constant shaking. Trypsin was added in a 1:50 ratio and the samples were incubated overnight (18 hours) at 37 °C with constant shaking. The next day, samples were added to the magnetic apparatus. The supernatant was removed and acidified with ~1% formic acid (pH 2) to inactivate trypsin. All monoclonal antibodies were processed in duplicate, including the CSPG4 positive control. The NIP negative control was processed in triplicate.

Liquid chromatography coupled to tandem mass spectrometry (LC-MS/MS): In all samples, peptides were extracted from solution using C18 OMIX tips (Agilent Technologies, Santa Clara, CA) and eluted in 3 µl of elution buffer B (65% acetonitrile, 0.1% formic acid). Fifty-seven µl of buffer A (0.1% formic acid) were added to each sample and 18 µl of sample was loaded from a 96-well microplate autosampler using the EASY-nLC 1000 system (Thermo Fisher Scientific) onto a 75 µm x 3.3 cm capillary (IntegraFrit Capillary, New Objective, Woburn, Massachusetts) packed-in-house with a C18 Agilent Pursuit 5 µm bead media (Agilent Technologies, Santa Clara, California). Peptides were eluted from the trap column at 300 nl/min with an increasing concentration of Buffer D (0.1% formic acid in 100% acetonitrile) over a 30 min gradient onto a resolving 15 cm x 75 µm ID analytical column (PicoFrit Capillary, New Objective) packed-in-house with C18 Agilent Pursuit 3 µm bead media (Agilent Technologies). The liquid chromatography setup was coupled online to Q Exactive H-FX (Thermo Fisher Scientific) mass spectrometer using the NanoSpray Flex

ionization source (Thermo Fisher Scientific) with the capillary temperature set to 320 °C and a spray voltage of 2kV. A 60 min data-dependent acquisition (DDA) method performed a full MS1 scan from 400–1500 m/z at a resolution of 70,000 in profile mode. This was followed by fragmentation of the top 12 parent ions using the HCD cell and detection of fragment ions at a resolution of 17,500. The following MS method parameters were used: MS1 Automatic Gain Control (AGC) target was set to 1e6 with maximum injection time (IT) of 50 ms; MS2 AGC was set to 5e4 with maximum IT of 110 ms; isolation window was 1.6 m/z; intensity threshold was 9.1e3; normalized collision energy (NCE) was set to 27; charge exclusion was set to fragment only 2+,3+, 4+ charge state ions; peptide match was set to preferred and dynamic exclusion was set to 18 s. Blank injections of buffer A (1 µl) were run between duplicates and reproducibility was confirmed by running 0.1 fmol/µl bovine serum albumin (BSA), every 10 runs.

Parallel reaction monitoring mass spectrometry (PRM-MS): Additionally, peptides extracted for LC-MS/MS analysis were analyzed using a targeted parallel reaction monitoring (PRM) MS approach. Samples were loaded (18 µl) onto a 3.2 cm C18 trap column (5 µm C18 particle, 150 µm inner diameter) using the using the EASY-nLC 1000 system (Thermo Fisher Scientific) running buffer A. Peptides were eluted from the trap column at 300 nl/min onto a resolving 15 cm long PicoTip Emitter (3 µm C18 particle) with an inner diameter of 75 µm (8 µm tip, New Objective). The LC setup was coupled online to a Q-Exactive Plus (Thermo Fisher Scientific) mass spectrometer with a nanoelectrospray ionization source. A 60 min DDA method was setup on the Q-Exactive Plus. The full MS1 scan from 400 to 1,500 m/z was acquired in the Orbitrap at a resolution of 70,000. AGC for MS1 was set to 1×10^6 with a maximum injection time of 120 ms. AGC target for MS2 was set to 2×10^5 with a maximum injection time of 130 ms, normalized collision energy (NCE) was set to 27. Reproducibility was confirmed by running a quality control solution of 0.1 fmol/µl BSA.

Data analysis: XCalibur software v.2.0.6 (Thermo Fisher Scientific) was used to generate raw files. Raw files were uploaded into Proteome Discoverer v. 1.4 (Thermo Fisher Scientific) and searched with Sequest HT search engine against the Human 5640 Swiss-Prot protein database (January 2018). Search parameters included trypsin (full) enzyme digestion, a maximum of two missed cleavages, static modification of cysteine carbamidomethylation, dynamic modification of methionine oxidation, precursor mass tolerance of 7 ppm, fragment mass tolerance of 0.02 Da, 1% false-discovery rate (FDR) at the peptide and protein level using the Percolator node.

Supplementary References

1. Bashford-Rogers RJM, Smith KGC, Thomas DC. Antibody repertoire analysis in polygenic autoimmune diseases. Immunology. 2018 Sep;155(1):3-17. doi: 10.1111/imm.12927. Epub 2018 Apr 16. PMID: 29574826; PMCID: PMC6099162.

2. Sanz I, Wei C, Jenks SA, Cashman KS, Tipton C, Woodruff MC, Hom J, Lee FE. Challenges and Opportunities for Consistent Classification of Human B Cell and Plasma Cell Populations. Front Immunol. 2019 Oct 18;10:2458. doi: 10.3389/fimmu.2019.02458